Geophysical Research Letters

Supporting Information for

Revealing a High Water Abundance in the Upper Mesosphere of Mars with ACS onboard TGO

Denis A. Belyaev[1], Anna A. Fedorova[1], Alexander Trokhimovskiy[1], Juan Alday[2], Franck Montmessin[3], Oleg I. Korablev[1], Franck Lefèvre[3], Andrey S. Patrakeev[1], Kevin S. Olsen[2], and Alexey V. Shakun[1]

[1]Space Research Institute (IKI), Moscow, Russia.

[2]Department of Physics, University of Oxford, UK.

[3]LATMOS/CNRS, Paris, France.

Corresponding author: Denis Belyaev (dbelyaev@iki.rssi.ru)

Contents of this file

Text S1 to S3: pages 2-4
Figures S1 to S4: pages 4-6

Introduction

The present Supporting Information describes details of the ACS MIR instrument and the concept of altitude profiles retrievals from the measured transmission spectra. The retrieval algorithm is supplemented by Figure S1, which demonstrates instrumental and temperature peculiarities of the CO_2 and H_2O absorption spectroscopy around 2.7 μm band (echelle order #223 of ACS MIR). Figure S2 shows validation of the derived temperature, H_2O number density and mixing ratio profiles for different seasonal scenarios in MY34. Latitudinal variation of the high altitude water around perihelion is presented in Figure S3 for both MY34 and MY35. Figure S4 presents vertical distribution of all data points for H_2O VMR in the GDS and perihelion seasons. Uncertainties of the obtained data are described separately in section Text S3.

Text S1. Instrument description

The middle infrared channel of the Atmospheric Chemistry Suite is a cross-dispersion echelle spectrometer dedicated to solar occultation measurements in the 2.3–4.3 μm wavelength range (Korablev et al., 2018). Each occultation session is devoted to one of ten angular positions of the MIR secondary grating that disperses about 10-20 echelle orders spatially separated and recorded simultaneously at the focal plane array (FPA) by 640x512 pixels. The spectral range of our interest, 2.66-2.68 μm, lies within the diffraction order #223 at the grating position #4. One order covers a spectral interval of about 30 cm^{-1} (~25 nm); a spectrum is dispersed along 640 FPA elements with the sampling of 0.05 cm^{-1} and the resolving power λ/δλ reaching ~25000 (δλ~0.15 cm^{-1}). In the occultation field of view (FOV), the instrumental rectangular slit cuts a part from the solar disk, so that one order occupies a stripe with about 20 FPA rows. In such a manner, the consequences of orders are located on the matrix as stripe-by-stripe, one above the other, with some dark rows between them. For our analysis, we selected a central row from the stripe correspondent to order #223 that provides the maximal signal-to-noise ratio.
The calibration procedure for the analyzed transmissions encompassed a pixel-to-wavenumber assignment and a determination of the instrument line shape (ILS). The procedure was applied for every occultation and in various spectral intervals separately since we observed variability of the light spreading over the FPA from orbit to orbit. Using strong CO_2 and H_2O absorption lines in order #223, we derived an optimal wavenumber assignment by a parabolic law and an asymmetric ILS including a superposition of two Gaussian functions (Fig. S1a). Previously, Alday et al. (2019) implemented an analogous approach for MIR spectra but in the grating position #5.

Text S2. Retrieval concept

A scheme for the water VMR retrieval consists of several iterations with a fitting of a forwardly modeled transmission spectrum to a measured one at each observed altitude. The forward modeling includes contributions from H_2O, HDO, and CO_2 molecular absorption cross-sections that are abundant in the 2.66-2.68 μm spectral range, i.e. 3730-3755 cm^{-1} (Fig. S1b). They were calculated using line-by-line modeling for specified temperatures and pressures on a basis of the HITRAN2016 database (Gordon et al., 2017) taking into account H_2O and HDO lines broadening in the CO_2-rich atmosphere (Gamache et al., 2016; Malathy Devi et al., 2017) and self-broadening in the case of CO_2. A transmission spectrum $J(\nu,T,p)$ is defined by the cross-sections $\sigma(\nu,T,p)$, gaseous concentrations $N_{mol} = f_{mol} \bullet p/k_B T$, and aerosol slant opacity τ_a. Here, ν is wavenumber; T and p are the atmospheric temperature and pressure respectively; f_{mol} – volume mixing ratio (VMR) of a molecule; k_B – Boltzmann constant. In order to fit such a synthetic spectrum J_{mod} to the measured one J_{mes}, we convolved the model by the previously derived ILS using wavenumber calibrations. The aerosol opacity $\tau_a = -log(J_a)$ was fitted from the measured transmission as a continuum level J_a out of molecular absorption.
The fitting procedure includes minimization of the function $\chi^2 = \sum_i A^2(\nu_i)$, which is a residuals sum over all considered spectral points i (pixels) divided by the transmission errors $\delta J(\nu_i)$, where $A(\nu_i) = \left(J_{mod}(\nu_i) - J_{mes}(\nu_i)\right)/\delta J(\nu_i)$. An optimal search for the minimum was based on Levenberg-Marquardt algorithm (Marquardt, 1963) with the Jacobian matrix containing transmission derivatives $[\partial A/\partial X]$ on free parameters X, i.e. T, N_{CO_2}, f_{H_2O} or τ_a. Here, the clue contribution comes from the partial cross-section derivative on temperature $\partial\sigma/\partial T$. It differs for each molecule from line to line with a change of sign as seen in the Figure S1c. Thanks to that, an independent and simultaneous retrieval of temperature and molecular concentrations is possible.

In our multi iteration scheme, the first step is devoted to temperature and pressure retrievals with the rotational structure of CO_2 absorption bands. They are selected out from strong H_2O and HDO lines, e.g. in intervals 3733-3735 cm^{-1}, 3738-3743 cm^{-1} of the order #223. Total number of spectral points exceeds 150 that makes the χ^2-minimization confidential. Altitude profiles $T_1(z)$ and $N_{CO2}(z)$ are directly retrieved, while the pressure is expressed on the first stage through the ideal gas law as $p_1(z) = \left({N_{CO2}(z)}/{f_{CO2}(z)}\right) k_B T_1(z)$. The CO_2 VMR vertical distribution $f_{CO2}(z)$ is taken from the Mars Climate Database (MCD) (Millour et al., 2018). Then, in order to meet the hydrostatic law, we constrain the pressure by a formula for the hydrostatic equilibrium, $p_{hyd}(z) = p_o exp\left[-\int_{z_o}^{z} \frac{g(h)M(h)}{k_B T_1(h)} dh\right]$, using the retrieved $T_1(z)$. Here, g is the gravity acceleration, M is the molecular weight (taken from MCD). A reference pressure $p_o = p(z_o)$ is selected at an altitude z_o, where the retrieval uncertainties are minimal. In all derived profiles, this level lies between 30 and 60 km corresponding to the deepest, but not saturated, absorption lines (see Fig. 1b). Once the hydrostatic pressure profile is calculated, we keep it fixed when a new temperature and CO_2 density are retrieved on the next step. We repeat this procedure about 4-5 iterations reaching the profiles convergence. Values on an $(i-1)^{th}$ step are used as a priori for the i^{th} one, while for the 1^{st} stage we take the values from MCD. Analogous hydrostatic approach has been recently verified by other temperature and pressure retrievals from the ACS data (Alday et al., 2019, 2021; Fedorova et al., 2020). On the last stage, we apply the temperature and density profiles as a reference atmosphere for the H_2O mixing ratio retrieval (Fig. S2c) in the wavenumber interval from 3743 to 3753 cm^{-1}. We do not fit the HDO concentration separately and keep it as 5 times of the terrestrial SMOW value (Standard Mean Ocean Water), which is $1.56 \cdot 10^{-4}$ for this isotope (Owen et al., 1988; Krasnopolsky, 2015). This assumption simplifies the fit, decreasing the number of free parameters, and it makes sense for the tiny detection of high altitude water. In parallel, each retrieval is accompanied by the derived aerosol opacity τ_a, which may characterize the dust activity during an occultation (see Figure 2a).

Examples of the derived temperature, H_2O number density and mixing ratio profiles are shown on Figure S2 in comparison with collocated and simultaneous occultations by the ACS near-IR channel (see in Fedorova et al. (2020)), as well as with the MCD predictions for particular occultations. The validation is demonstrated for three orbits that correspond to different atmospheric scenarios in MY34: before GDS (L_S 164°), during GDS (L_S 196.6°) and close to perihelion (L_S 260.9°). Sensitivity of the NIR spectroscopy does not allow measuring temperature and densities above 100 km. In the MIR case, one can potentially retrieve the temperature altitude profiles spreading from 10-40 km (depending on aerosol opacity) up to 150 km in the considered spectral range (Fig. S2a). The upper altitude of the water detection is 20-25 km higher for the 2.66-2.67 μm band in MIR than 1.38 μm in NIR (Fig. S2b, S2c).

Text S3. Estimation of uncertainties

The transmission errors δJ, included in the Jacobian matrix, determine uncertainties of the retrievals for each of free parameters. We estimated them for any observed altitude as a multiplication of the derivatives array by the transposed one, $\delta X = \sqrt{[\frac{\partial A}{\partial X}] \times [\frac{\partial A}{\partial X}]'}$, over the spectral points. The error bars δJ are composed of a statistical noise and some systematic uncertainties. We derived the statistical noise analyzing transmission fluctuations near 1 at altitudes above 200 km. It gave the standard deviation of about $5 \cdot 10^{-4}$ for a signal recorded in the considered FPA row and in the center of the range, 3735-3750 cm^{-1}. The systematics comes

from the obtained calibrations (wavenumber, ILS) and from the hydrostatic pressure and temperature uncertainties when modeling transmission spectra on the final step of H_2O VMR retrievals. On average, it increases the δJ value up to 0.001-0.0015. The described uncertainties establish a detection limit of $5 \cdot 10^6$-$1 \cdot 10^7$ cm^{-3} for H_2O number density above 100 km. When the water enrichment exceeds this order of magnitude, we observe a positive detection of the molecular abundance at high altitudes. In the opposite case, an upper limit is determined (see Fig. 1c).

Supplementing Figures:

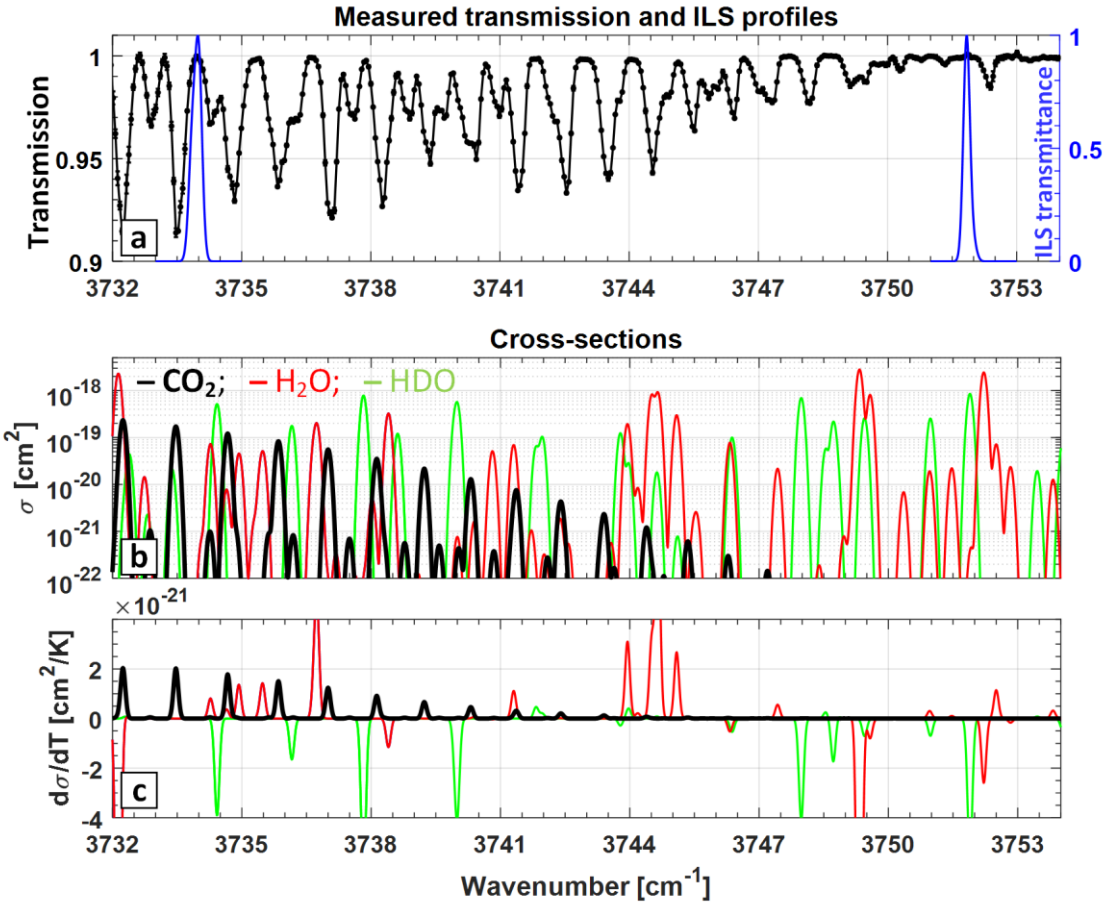

Figure S1. Absorption spectroscopy in the echelle order #223 of ACS MIR. **a**: Example of measured transmission spectrum at a target altitude of 100 km (black axis) and the instrumental line shape (ILS) for both edges of the considered wavenumber range (blue axis). **b**: Absorption cross-sections for molecules CO_2 (black), H_2O (red), and HDO (green) calculated for T=150 K and p=10^{-5} mbar and convolved by ILS. **c**: Partial temperature derivatives of the considered cross-sections.

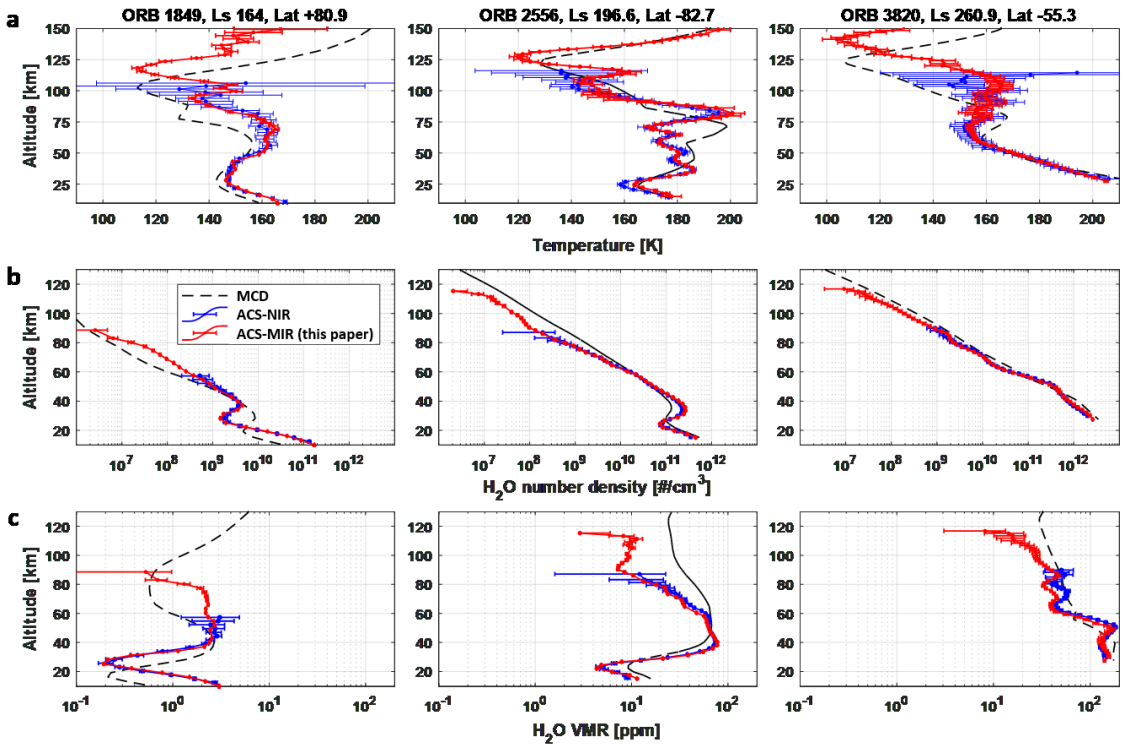

Figure S2. Validation of vertical profiles retrieved by ACS-MIR (red) with analogous profiles of ACS-NIR (from Fedorova et. al, 2020) (blue) and with predictions of MCD (Millour et al., 2018) (black): (**a**) temperature; (**b**) H_2O number density; (**c**) H_2O volume mixing ratio (VMR).

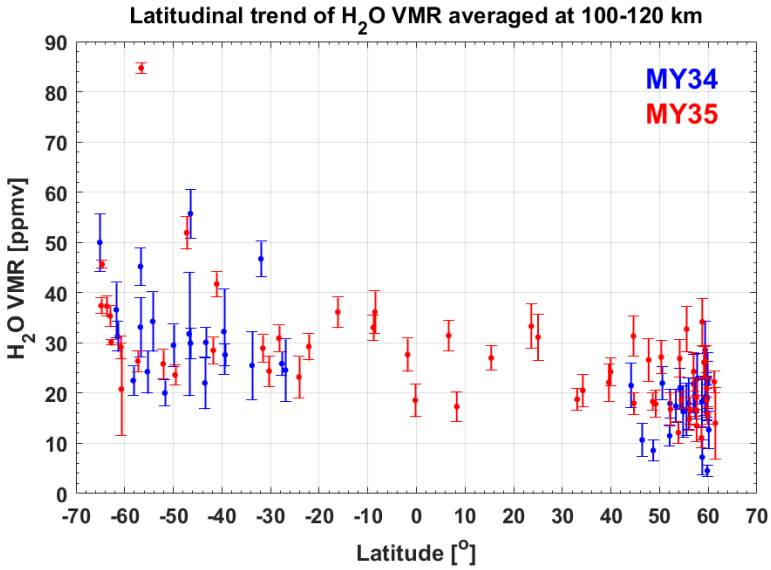

Figure S3. Latitudinal trend of H2O volume mixing ratio (VMR) in the perihelion seasons (Ls 250°–295°) of MY34 (blue) and MY35 (red). Each individual point is a weighted mean value revealed over altitude range of 100-120 km from a vertical profile of water VMR.

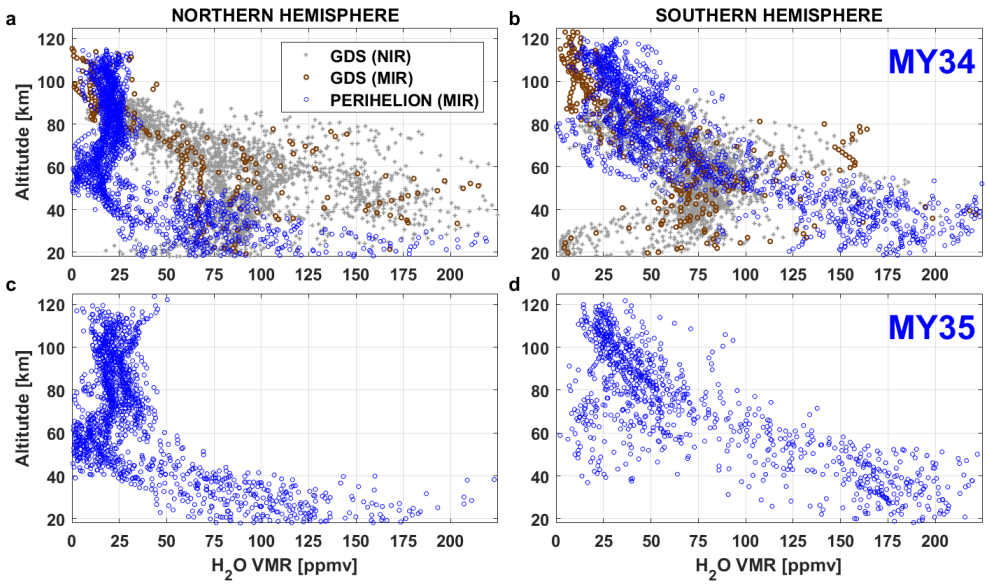

Figure S4. Altitude distribution of H_2O volume mixing ratio (VMR) during the GDS (MY 34) and the perihelion season (MY 34, 35). The dataset used includes all ACS MIR observations at GDS of MY34 (L_S=195°–220°) (brown) and around the perihelion point (L_S=250°–295°) (blue). Panels (a, b) for MY34 and (c, d) for MY35 from the Northern (a, c) and Southern (b, d) hemispheres. Light grey points are the NIR data during GDS of MY34 (Fedorova et al., 2020).